Influence of vision measurement system spatial configuration on measurement uncertainty, based on the example of electric traction application.

1. Introduction

Approximately 900 thousand kilometres of railway lines are currently exploited in the world. Passenger services worldwide reach almost 3.5 billion pkm ($3.5 \cdot 10^{12}$), while cargo services are at the level of 10 billion tkm ($10 \cdot 10^{12}$) and rising. More than 40% of railway lines in the world are electrified. In Europe this index reaches 50%, in Poland 60.5%, while in Switzerland it is 100%. In the case of electrified railway lines damage to the supply system and the contact line results in significant transport difficulties and generates considerable losses. This is the reason why periodical control of technical condition of the overhead contact line (OCL) is necessary, in order to ensure reliability and safety of railway transport systems. In many countries such inspection is performed in a traditional way, i.e. by visual control performed by employees of the infrastructure operator. Such approach is time-consuming, generates breaks in normal functioning of the route and, first and foremost, depends heavily on the subjective assessment of a given inspector. Monitoring the condition of the contact line has been greatly improved by implementing into exploitation diagnostic systems mounted on selected cars and/or vehicles, which can move at the speed allowed for a given railway line [1, 2]. The scope of conducted diagnostics includes the so-called static characteristics, i.e. measurement realised without taking into consideration the impact of a current collector on the contact line, as well as the assessment of dynamic quality of the interaction between the two elements for the allowed exploitation velocity. Originally all measurements were performed with the use of so-called measuring current collectors, which introduces certain limitations in the case of assessing static parameters. In order to minimise the influence of dynamic compounds on the measurement, the speed of diagnostic vehicles was reduced. As a result, the time necessary to inspect a given section was visibly shortened when compared to manual inspection; on the other hand, the line capacity was limited. The disadvantages of contact systems are eliminated in contact-less techniques, where an important role is played by visual systems.

There are two main solutions which may be applied in monitoring the technical condition of the contact line. The dominating one is to use a visual system to analyse cooperation between the contact line and a current collector through which the current supplying the vehicle is passing. Such systems can be exploited on vehicles participating in normal traffic, which constitutes their significant advantage. However, in accordance with the provisions of the Technical Specifications for Interoperability and, consistently, in the norm EN-50317, the important factors in assessing the quality of dynamic cooperation OCL-current collector are: the simultaneous measurement of the so-called contact force together with the contact wire uplift at the support as the pantograph passes the suspension point or the measurement of the so-called percentage of arcing (NQ). In the case of measuring the NQ either detectors of radiation accompanying arcing [3] or thermovision [4] are applied. Algorithms allowing for automatic detection of light flashes associated with electric arc [5] are proposed with regard to visual systems recording images within the scope of visible radiation. The above-mentioned methods do not allow for detection of arc-free gaps. This is why simultaneous analysis of an image, correlated with analysis of the current taken by a vehicle [6] is often used. In practical system the assessment of quality of dynamic cooperation between the overhead contact line and a current collector is performed more often by way of measuring contact force and the contact wire uplift at the suspension point. Usually the measurement of force is realised with the use of sensor methods, although it is also possible to employ visual techniques [7]. The way of measuring height changes at the suspension point, realised from the vehicle's point of view, has been presented in numerous papers. It is possible to distinguish the methods for dynamic

assessment of stagger, described in [8, 9] and the solutions appropriate in the light of normative requirements, presented in [10, 11, 12].

Systems for measuring static parameters, where the leading role is played by visual systems which do not require the presence of a measuring and/or working collector [13, 14, 15] constitute a separate group of solutions. The analysis of applied methods shows that the main focus is on improving the algorithms used for automatic analysis of an image, often recorded in dynamic lighting conditions [16, 17, 18, 19]. Within the area of measurements for traction applications, there is no analysis of measurement uncertainty. It is crucial in specific measurement conditions, where the displacement of contact line elements at the level of a few dozen and/or a few hundred millimetres are registered, for safety reasons, from the distance ranging between a few dozen centimetres and/or a few metres. It should be stressed that the measurement resolution usually presented is that which is possible to obtain, while the defined error is either the maximum one, an average one or the RMS one, without any details as to how and with the use of which measurement tools it has been obtained [9, 15]. Such approach is useless, as far as metrology is concerned, unless the applied system serves to perform the quality rather than quantity assessment, as has been presented, for example in [5].

The aim of this research is to define measurement uncertainty with regard to the position of an object in motion, with the use of visual technique. It is assumed that the outer dimensions of the object correspond to a typical cross-section of contact wire and that it may move at two degrees of freedom, within the scope corresponding to typical dynamic movements of the contact line, caused by the passing current collector (Fig. 1).
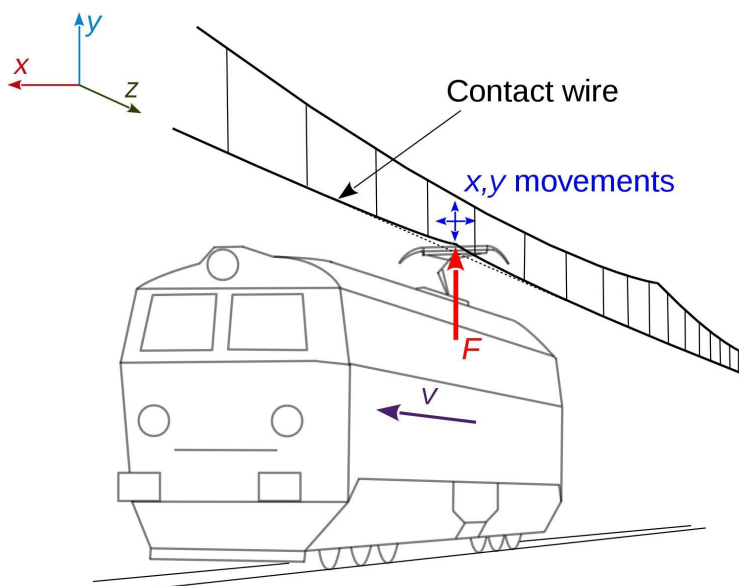

Fig. 1. Dynamic movements of contact wire caused by a passing current collector

The research was focused on analysing the influence of measurable geometric parameters, which unambiguously define the relative position of the camera and the tested object. The proposed new method does not require a calibration procedure; it is only necessary to measure geometrical values at the stage of construction of the measurement system. In particular, such approach is less dependent on external factors, such as significantly different lighting conditions at the calibration in relation to the place where the measurements are performed. Experimental tests have shown that measurement uncertainties obtained with the use of the proposed approach are sufficient for both diagnostic and laboratory measurements.

2. Uncertainty in measuring geometrical parameters with the use of visual methods

The uncertainty in measuring geometrical parameters with the use of visual methods may be generally divided into internal and external, i.e. dependent on and independent of the camera [20]. The factors affecting this type of measurement, which are most often taken into consideration include the following:

   a) Limitations of optics, e.g. distortion or aberration. The deformations caused by distortion have been analysed in literature on numerous occasions. They are usually corrected by introducing a multi-nominal model [21].
   b) Limitations of the bandwidth connected with the time necessary to generate and transmit the image from the camera to the computer [22].
   c) Limitations of algorithms for image transformation, resulting both from the efficiency indicator and from the transformation time [22, 23].
   d) Lighting limitations arising mostly from restricted possibilities to ensure constant, clearly defined lighting parameters for the observed scene [24].
   e) Resolution limitations resulting from the applied image converter [22, 25].

The above factors are usually not taken into consideration simultaneously. This results from the variety of configurations of the applied visual measurement systems. For the purposes of the conducted research it has been assumed, through ensuring certain parameters at the stage of designing a research stand, that only the influence of spatial configuration and its defined geometric dimensions will be subjected to analysis. There is no comprehensive approach to this kind of analysis in the available literature. In the elaborations [13, 14, 26] the analysis was performed only for one spatial configuration.

3. Variants of spatial configuration of the system for dynamic measurements of the overhead contact line geometry

The basic requirement for geometrical configuration of a system measuring dynamic displacements of contact line wires by an optical method with the use of a video camera and image analysis is the possibility to record both horizontal and vertical displacements.

Having assumed that the above paramount requirements is fulfilled, the measurement of contact line vibrations may be performed, particularly under field measurement conditions, for two basic geometrical configurations of the measurement system. In the first case, the camera is placed at the same height as the examined element and records the image at a sharp angle in relation to this element of the contact line. The second variant is different from the first one in that the camera is not placed at the height of the examined element, but either above or below it, which makes it necessary to position the camera at a certain angle in relation to the level.

In the course of the analysis, the above variants will be compared with a third, theoretical one, in which the camera would be placed on the axe of the examined element of the contact line (e.g. the contact wire). Using this variant to measure vibration parameters of a real object is impossible for obvious reasons, unless the examination concerns a short section of the contact wire, fixed at one end and stimulated to vibrate. Such measurements may be used in order to identify the parameters of contact line for modelling purposes. This variant is characterised by the lowest level of uncertainty, and therefore will be used as reference for the remaining two spatial configurations of the measurement system.

The individual variants of measurement system configuration are described in detail in the following part of this paper. While discussing all the configurations, only the measurable values were taken into consideration, i.e. the ones which can be measured or established based on other measurements, with definable uncertainty.

3.1. En face measurement – baseline option

Spatial configuration for horizontal displacements during the measurement has been shown in Fig. 2. The variant for vertical displacement looks identically.
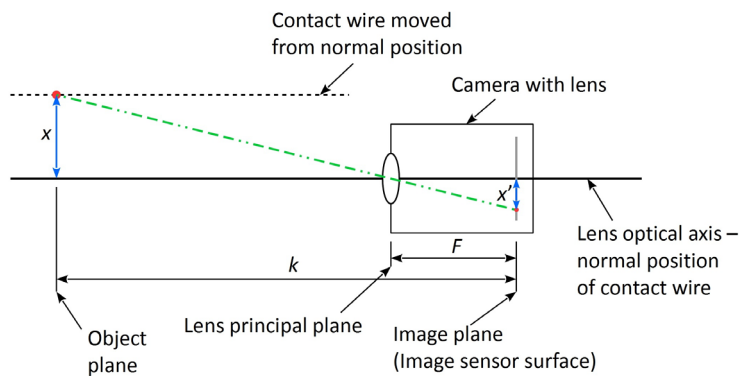

Fig. 2. Spatial configuration during en face measurement (view from above)

During the en face measurement the image plane (i.e. the matrix plane) and the plane in which the object whose position is measured is moving, are parallel to each other. Hence there are no geometrical disfigurements of the image connected with perspective, and the mathematical dependence, representing real changes in the position of an object in horizontal axis, based on the changes in its position on the camera matrix, taking into consideration only the measurable values, is given by the following dependence (1):

$$x = x' \cdot \left(\frac{k}{F} - 1\right) \quad (1)$$

where: k – distance between object plane and image plane; F – distance between optical centre of lens and image plane; x' – displacement of the image on the camera matrix in the horizontal axis.

Due to the parallelism of the object plane and the image plane, the analogous dependence applies to vertical displacements (2):

$$y = y' \cdot \left(\frac{k}{F} - 1\right) \quad (2)$$

where: ; y' – displacement of the image on the camera matrix in the vertical axis.

The distance F between the optical centre of the lens and the image plane depends on the focal length of the lens and on the reproduction ratio and is given by the following dependence (3):

$$F = \frac{k - \sqrt{k^2 - 4 \cdot k \cdot f}}{2} \quad (3)$$

where: f – focal length of lens.

The focal length of lens f, even in the case of fixed lens, is not a constant value, but changes slightly, depending on the current focus. Here we observe the effect of the so-called floating focal length. This effect has to be taken into consideration, therefore the focal length of the lens is established based on an additional measurement, for the current focus of the lens, in accordance with the following formula (4):

$$f = \frac{k}{2 + \frac{x'_w}{x_w} + \frac{x_w}{x'_w}} \quad (4)$$

where: x_w – the size of the model with known dimensions; x_w' – the size of the model image on the camera matrix

As it can be observed, in the case of en face measurement, the measured values of displacement in horizontal and vertical axes are independent of each other, i.e. the x value depends solely on the variable x', and y, respectively, on y'.

3.2. Side measurement at the alpha angle

Spatial configuration during the measurement of horizontal displacements of contact line elements in the side variant has been presented in Fig. 3.
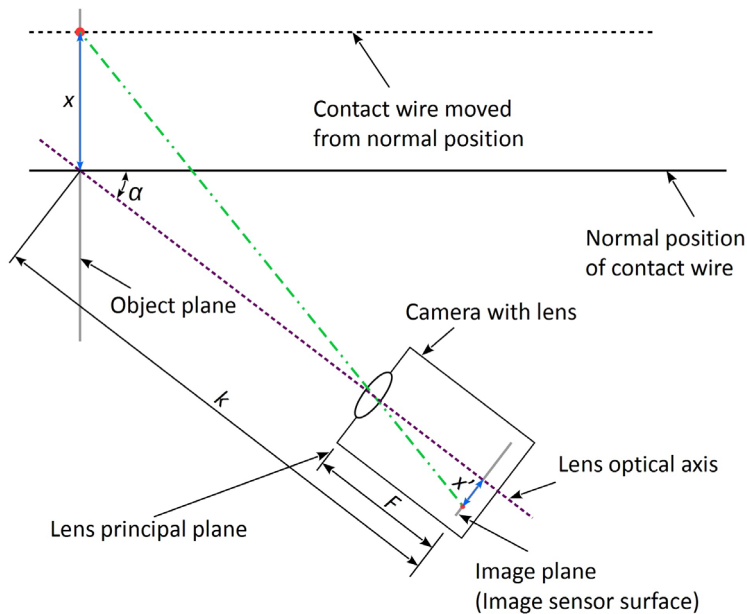

Fig. 3. Spatial configuration for measurement in side variant (view from above)

As it can be observed, the camera is pointed at the element of the contact line from one side, at the angle α, and because of that the object plane and the image plane are not parallel to each other. As a result, the image recorded in the object plane is vitiated by single trapezoidal distortions. In this case k is the distance between the image plane and the central point of the object plane. Taking into consideration only the measurable values, the mathematical dependence reproducing the object movement in the horizontal axis of the image plane, based on the position of the object image on the camera matrix, is given by the following formula (5):

$$x = \frac{x' \cdot (k-F)}{F \cdot cos\alpha - x' \cdot sin\alpha} \quad (5)$$

Analogously, for vertical movements, we have (6):

$$y = \frac{y' \cdot (k-F)}{F - x' \cdot tan\alpha} \quad (6)$$

With regard to measurements performed for this configuration, the results of horizontal displacements depend solely on the horizontal position of the image – x'. For vertical displacements, due to single trapezoidal distortions, the result depends both on displacements in the vertical and horizontal axes of the image (x' and y').

3.3. Sidelong measurements at alpha and beta angles

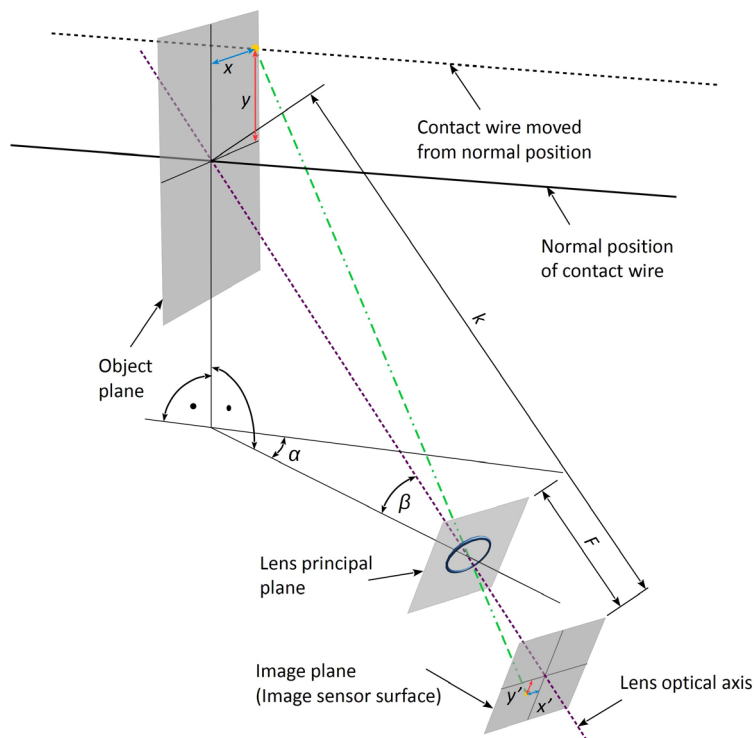Spatial configuration for measurements performed sideways has been presented in Fig. 4.

Fig. 4. Spatial configuration for sidelong measurements

As it can be observed, in sidelong measurements the camera is tilted from the element of the contact line at the angle α and inclined to the level at the angle β. The optical reproduction of the object plane on the matrix surface will therefore be characterised by double trapezoidal distortions. In such conditions, taking into consideration only measurable values, the dependence reproducing the object movement in the horizontal axis, based on the position of its image on the matrix surface, is given by the following dependence (7):

$$x = \frac{(k-F)\cdot x'\cdot cos\beta}{cos\alpha\cdot(F\cdot cos\beta - y'\cdot sin\beta) - x'\cdot sin\alpha} \quad (7)$$

An analogous dependence for the vertical axis looks as follows (8):

$$y = \frac{(k-F)\cdot(y' + x'\cdot sin\beta\cdot tan\alpha)}{F\cdot cos\beta - y'\cdot sin\beta - x'\cdot tan\alpha} \quad (8)$$

Due to the presence of double trapezoidal distortions, the object displacements, both in the vertical and in horizontal axis, depend on the position of this object's image in the vertical axis y' and the horizontal axis x'. In order to illustrate the issue more clearly, Fig. 5 shows characteristic reproduction of the object plane for all the measurement variants.
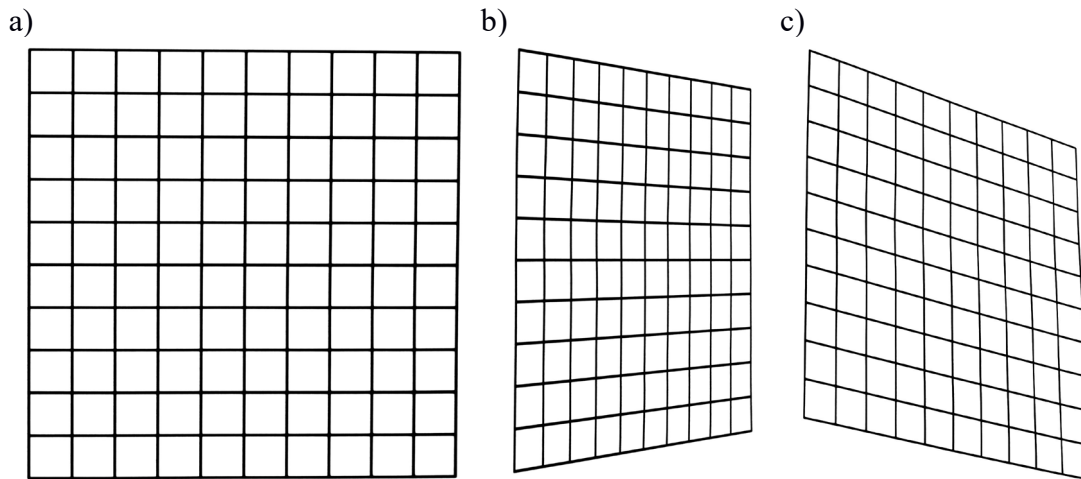
Fig. 5. Reproduction of object plane, where: a) en face measurement – no distortions; b) side measurement – single trapezoidal distortions; c) sidelong measurements – double trapezoidal distortions

4. The issue of measurement uncertainty for individual measurement configurations

Measurement uncertainty is one of the most underestimated engineering problems, and concerns all measurement areas. Due to the complexity of this issue, particularly in the case of multiple intermediate measurements, it is very often disregarded by the persons who perform the measurements. As a result, the obtained results have low value in use. With regard to the matter discussed here, the final measurement uncertainty depends both on constant values, resulting from the geometrical configuration of the system, and on variables, which arise from current changes of the element position, measured in the object plane. Depending on the configuration variant, the measurement uncertainty is related to the smaller or greater number of partial measurements, where some of them are already the result of indirect measurement. For the en face measurement it will be (9, 10):

$$u(x) = f\big(u(k); u(F); u(x')\big) \ (9)$$
and
$$u(y) = f\big(u(k); u(F); u(y')\big) \ (10)$$

Analogously, for side measurements we will obtain (11, 12):

$$u(x) = f\big(u(k); u(F); u(x'); u(\alpha)\big) \ (11)$$
and
$$u(y) = f\big(u(k); u(F); u(x'); u(y'); u(\alpha)\big) \ (12)$$

while in the case of sidelong measurement, the measurement uncertainties will be dependent on (13, 14):

$$u(x) = f\big(u(k); u(F); u(x'); u(y'); u(\alpha); u(\beta)\big) \ (13)$$
and
$$u(y) = f\big(u(k); u(F); u(x'); u(y'); u(\alpha); u(\beta)\big) \ (14)$$

In each case the uncertainty $u(F)$ is the indirect measurement uncertainty.

The more complex the configuration of the measurement system, the greater the number of indirect measurements affecting the final uncertainty of the result. Therefore it can be initially assumed that the lowest level of uncertainty will be obtained for the en face configuration, a slightly higher one – for side measurements, and that the worst situation will occur during sidelong measurements. Naturally, it will be true if we assume that, in all the cases, instruments with the same level of calibration uncertainty will be used for the measurement of the same values.

Analysis of the angle value influence on the uncertainty of measurement results, for individual spatial configurations, will be presented in the further part of this paper. These uncertainties will be compared with those obtained for reference configurations (en face measurement). The acceptable level of measurement uncertainty, as well as the threshold values of α and β angles, at which the reliability of the obtained results is not unacceptably deteriorated will be defined.

4.1. Sensitivity coefficients

Sensitivity coefficients define the influence of individual uncertainties of partial measurements on the result uncertainty. This section presents the analysis of dependence between sensitivity coefficients and variable parameters in individual measurement configurations. The analysis was performed on assumption that, for all the configurations, the distance k between the central point of the object plane and the image plane remains unchanged, and an identical reproduction ratio, i.e. the F distance between the lens plane and the image plane, is maintained. The scope of the measured displacements for all the cases has been assumed at the level ±120 mm, both with regard to the horizontal and the vertical axis. This scope corresponds to typical possible displacements of the contact wire. For side and sidelong measurement variants, in order to examine the influence of the angle value on uncertainty, it has been assumes that, both for the angle α and β, the range of change is from 5º to 75º. Typical laboratory measurement instruments have been used to measure individual values. The list of partial measurements, together with the obtained standard uncertainties, can be found in Table 1.

Table 1. Partial measurements with the obtained uncertainties

No.	Measured value	Measurement instrument	Instrument calibration uncertainty	Measurement result / scope of changes	Standard uncertainty
1	Distance k between image plane and object plane	1st class accuracy gauge Hultafors CC10M B	$\pm(0.1+0.1\cdot L)$ mm*	952.50 mm	±0.12 mm
2	Distance F between main lens plane and image plane	Indirect measurement	-	39.584 mm	±0.065 mm
3	Measurement of object image position on matrix x' and y'	Basler camera acA 2040-180kc	±0.0076 mm**	From -5.6250 to +5.6250 mm	±0.0044 mm
4	Angle α between camera and contact wire	Precise mechanical protractor FWP MKMb	$\pm0.05º$	From 5.000 to 75.000º	$\pm0.029º$
5	Angle β of camera inclination in relation to level	Inclinometer ACS-080-2-SC00-HE2-2W	$\pm0.1º$	From 5.000 to 75.000º	$\pm0.058º$
*L – measurement result in metres, rounded up to a full number of metres ** Uncertainty obtained based of standard deviation of measurement result stochastic spread, for stationary object examined with the use of extension factor equal 3.					

4.1.1. En face measurement

During the en face measurement there is symmetry between the measurements of displacement in vertical and horizontal axes. Therefore the analysis of sensitivity coefficients is identical for both measurements. This is why only the solution for the horizontal axis will be shown below. Sensitivity coefficients are given by the following dependencies (15–17):

- measurement of the k distance:

$$\frac{\partial x}{\partial k} = \frac{x'}{F} \ (15)$$

- measurement of the F distance:

$$\frac{\partial x}{\partial F} = \frac{-x' \cdot k}{F^2} \ (16)$$

- measurement of the position of a point on the matrix surface x':

$$\frac{\partial x}{\partial x'} = \frac{k}{F} - 1 \ (17)$$

For the values of partial measurements given in Table 1, the values of sensitivity coefficients for the en face measurement variant have been shown in Fig. 6.
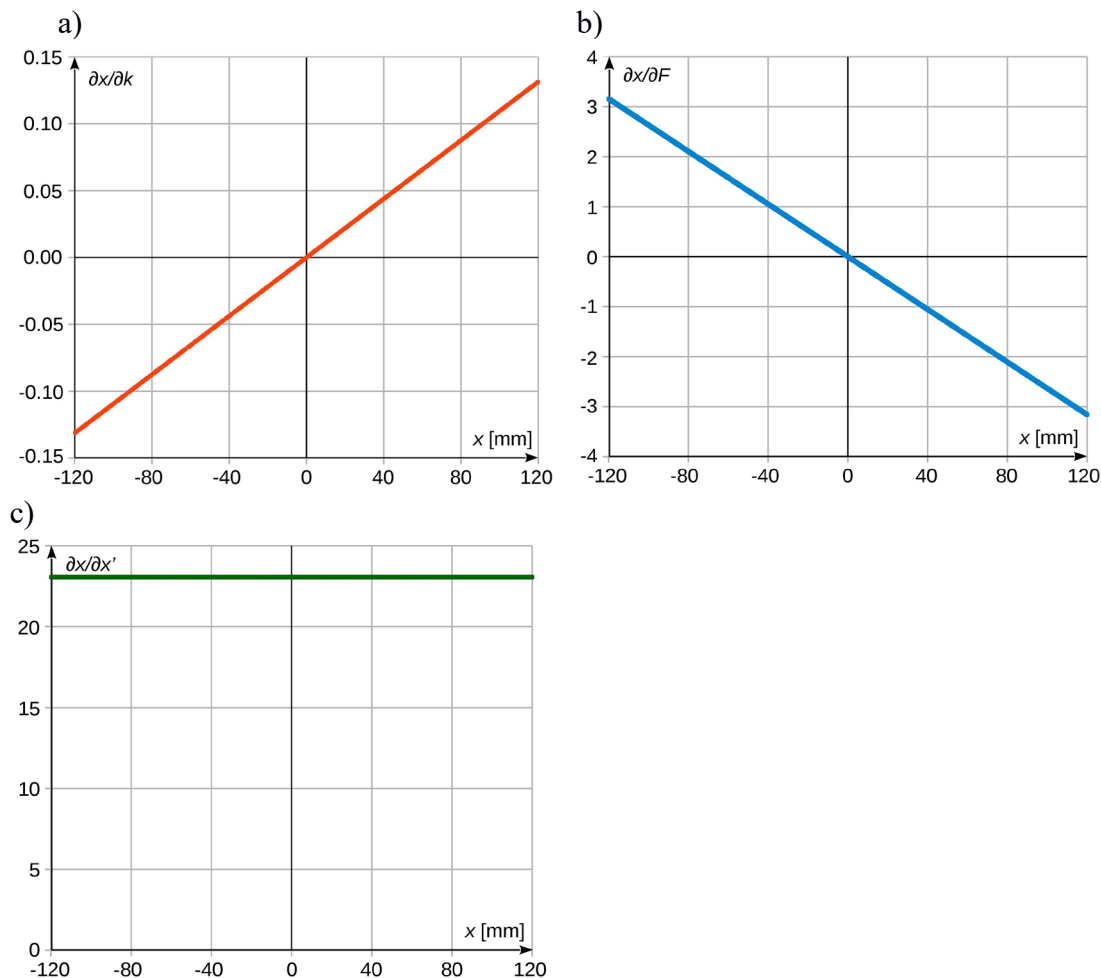
Fig. 6. Sensitivity coefficients for en face measurement, where: a) measurement of distance k; b) measurement of distance F; c) measurement of point position on matrix surface x'

4.1.2. Side measurement

During side measurements there occur single trapezoidal distortions. The dependence on horizontal displacements is related to four values, and in the case of vertical displacements – on five values.

For the measurement of displacements in the horizontal axis, the sensitivity coefficients are given by the following dependencies (18 – 21):

- measurement of the k distance:

$$\frac{\partial x}{\partial k} = \frac{x'}{F \cdot cos\alpha - x' \cdot sin\alpha} \quad (18)$$

- measurement of the F distance:

$$\frac{\partial x}{\partial F} = \frac{x' \cdot (x' \cdot sin\alpha - k \cdot cos\alpha)}{(F \cdot cos\alpha - x' \cdot sin\alpha)^2} \quad (19)$$

- measurement of the position of a point on the matrix surface x':

$$\frac{\partial x}{\partial x'} = \frac{F \cdot cos\alpha \cdot (k - F)}{(F \cdot cos\alpha - x' \cdot sin\alpha)^2} \quad (20)$$

- measurement of the α angle:

$$\frac{\partial x}{\partial \alpha} = \frac{x' \cdot (k - F) \cdot (F \cdot sin\alpha + x' \cdot cos\alpha)}{(F \cdot cos\alpha - x' \cdot sin\alpha)^2} \quad (21)$$

For the values of partial measurements given in Table 1, the values of sensitivity coefficients during the measurement of horizontal displacements for the side measurement variant have been shown in Fig. 7.
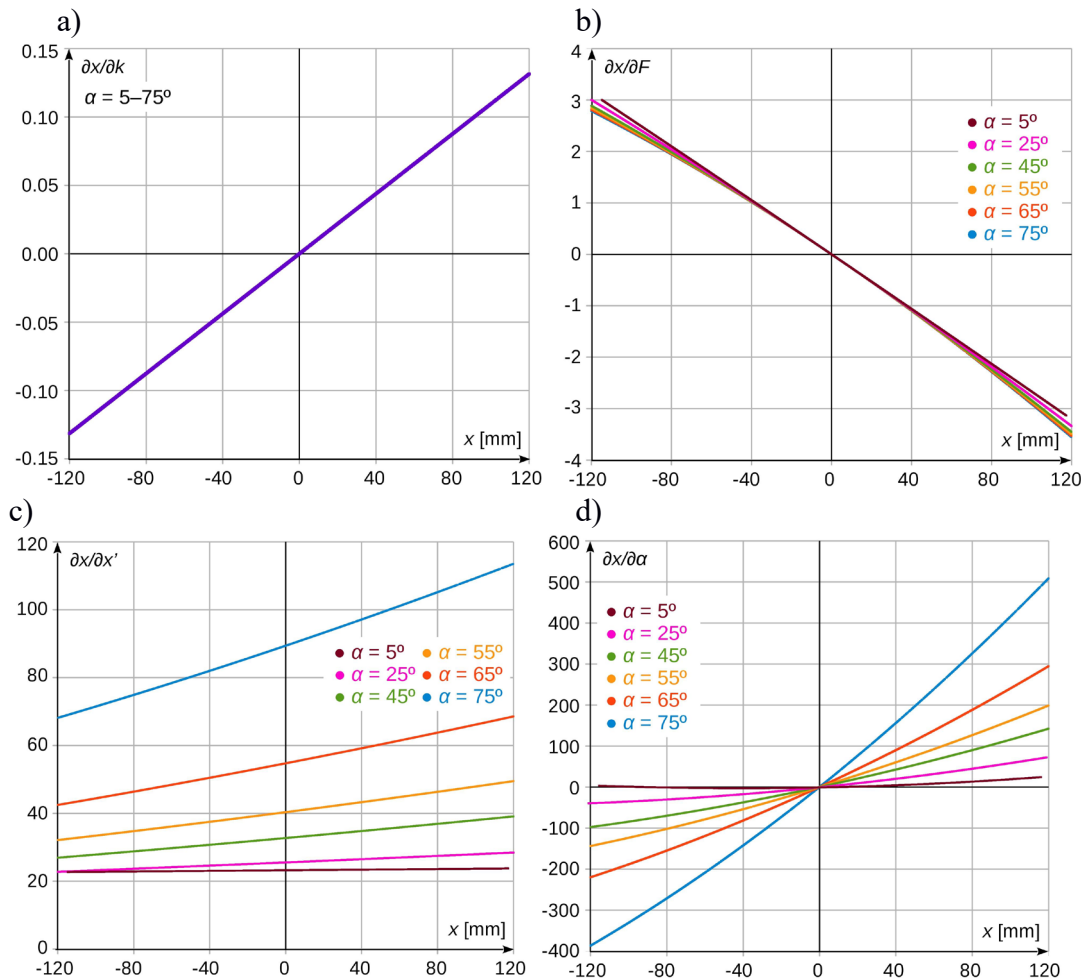

Fig. 7. Sensitivity coefficients for measurements in horizontal axis for side measurement, where: a) measurement of distance k; b) measurement of distance F; c) measurement of point position on matrix surface x'; d) measurement of angle α

Respectively, for the displacement in vertical axis, the sensitivity coefficients for individual measured values are given by the following dependencies (22 – 26):
- measurement of the k distance:

$$\frac{\partial y}{\partial k} = \frac{y'}{F - x' \cdot tan\alpha} \ (22)$$

-measurement of the F distance:

$$\frac{\partial y}{\partial F} = \frac{y' \cdot (x' \cdot tan\alpha - k)}{(F - x' \cdot tan\alpha)^2} \ (23)$$

- measurement of the position of a point on the matrix surface in the horizontal axis x':

$$\frac{\partial y}{\partial x'} = \frac{y' \cdot (k - F) \cdot tan\alpha}{(F - x' \cdot tan\alpha)^2} \ (24)$$

-measurement of the position of a point on the matrix surface in the vertical axis y':

$$\frac{\partial y}{\partial y'} = \frac{(k - F)}{F - x' \cdot tan\alpha} \ (25)$$

measurement of the α angle:

$$\frac{\partial y}{\partial \alpha} = \frac{y' \cdot x' \cdot (k - F) \cdot sec^2\alpha}{(F - x' \cdot tan\alpha)^2} \ (26)$$

For the values of indirect measurements given in Table 1, the values of sensitivity coefficients during the measurement of vertical displacements for the side measurement variant have been shown in Fig. 8.
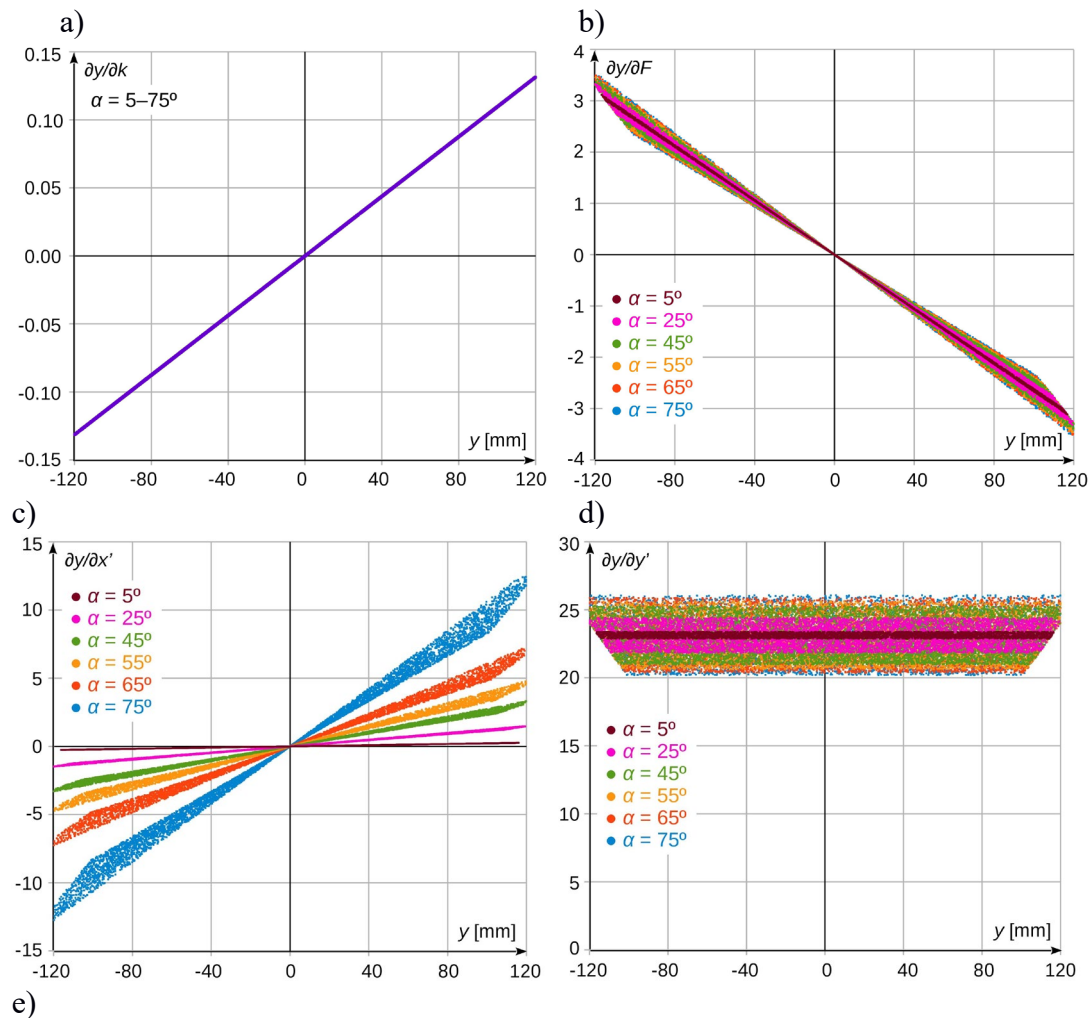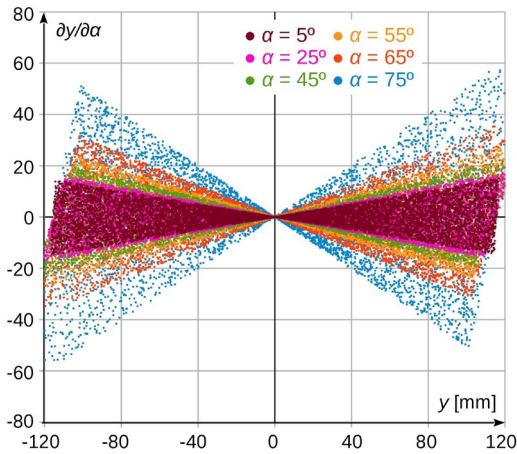
Fig. 8. Sensitivity coefficients for measurement in vertical axis in side measurement variant, where: a) measurement of distance *k*; b) measurement of distance *F*; c) measurement of point position on matrix surface in horizontal axis *x'*; d) measurement of point position on matrix surface in vertical axis *y'*; e) measurement of angle *α*

4.1.3. Sidelong measurement

For double trapezoidal distortions occurring during the sidelong measurement, the results of displacement measurement in both axes depend on six indirect measurements. The sensitivity coefficients for measurements in the horizontal axis are given by the following dependencies:

- measurement of the *k* distance (27 – 32):

$$\frac{\partial x}{\partial k} = \frac{x' \cdot cos\beta}{cos\alpha \cdot (F \cdot cos\beta - y' \cdot sin\beta) - x' \cdot sin\alpha} \ (27)$$

- measurement of the *F* distance:

$$\frac{\partial x}{\partial F} = \frac{x' \cdot cos\beta \cdot [cos\alpha \cdot (y' \cdot sin\beta - k \cdot cos\beta) + x' \cdot sin\alpha]}{[cos\alpha \cdot (F \cdot cos\beta - y' \cdot sin\beta) - x' \cdot sin\alpha]^2} \ (28)$$

- measurement of the position of a point on the matrix surface in the horizontal axis *x'*:

$$\frac{\partial x}{\partial x'} = \frac{(k-F) \cdot cos\beta \cdot cos\alpha \cdot (F \cdot cos\beta - y' \cdot sin\beta)}{[cos\alpha \cdot (F \cdot cos\beta - y' \cdot sin\beta) - x' \cdot sin\alpha]^2} \ (29)$$

- measurement of the position of a point on the matrix surface in the vertical axis *y'*:

$$\frac{\partial x}{\partial y'} = \frac{0.5 \cdot (k-F) \cdot x' \cdot cos\alpha \cdot sin2\beta}{[cos\alpha \cdot (F \cdot cos\beta - y' \cdot sin\beta) - x' \cdot sin\alpha]^2} \ (30)$$

- measurement of the *α* angle:

$$\frac{\partial x}{\partial \alpha} = \frac{(k-F) \cdot x' \cdot cos\beta \cdot [sin\alpha \cdot (F \cdot cos\beta - y' \cdot sin\beta) + x' \cdot cos\alpha]}{[cos\alpha \cdot (F \cdot cos\beta - y' \cdot sin\beta) - x' \cdot sin\alpha]^2} \ (31)$$

- measurement of the *β* angle:

$$\frac{\partial x}{\partial \beta} = \frac{(k-F) \cdot x' \cdot (y' \cdot cos\alpha + x' \cdot sin\alpha \cdot sin\beta)}{[cos\alpha \cdot (F \cdot cos\beta - y' \cdot sin\beta) - x' \cdot sin\alpha]^2} \ (32)$$

For the values of partial measurements given in Table 1, the values of sensitivity coefficients during the measurement of horizontal displacements for the sidelong measurement variant have been shown in Fig. 9.
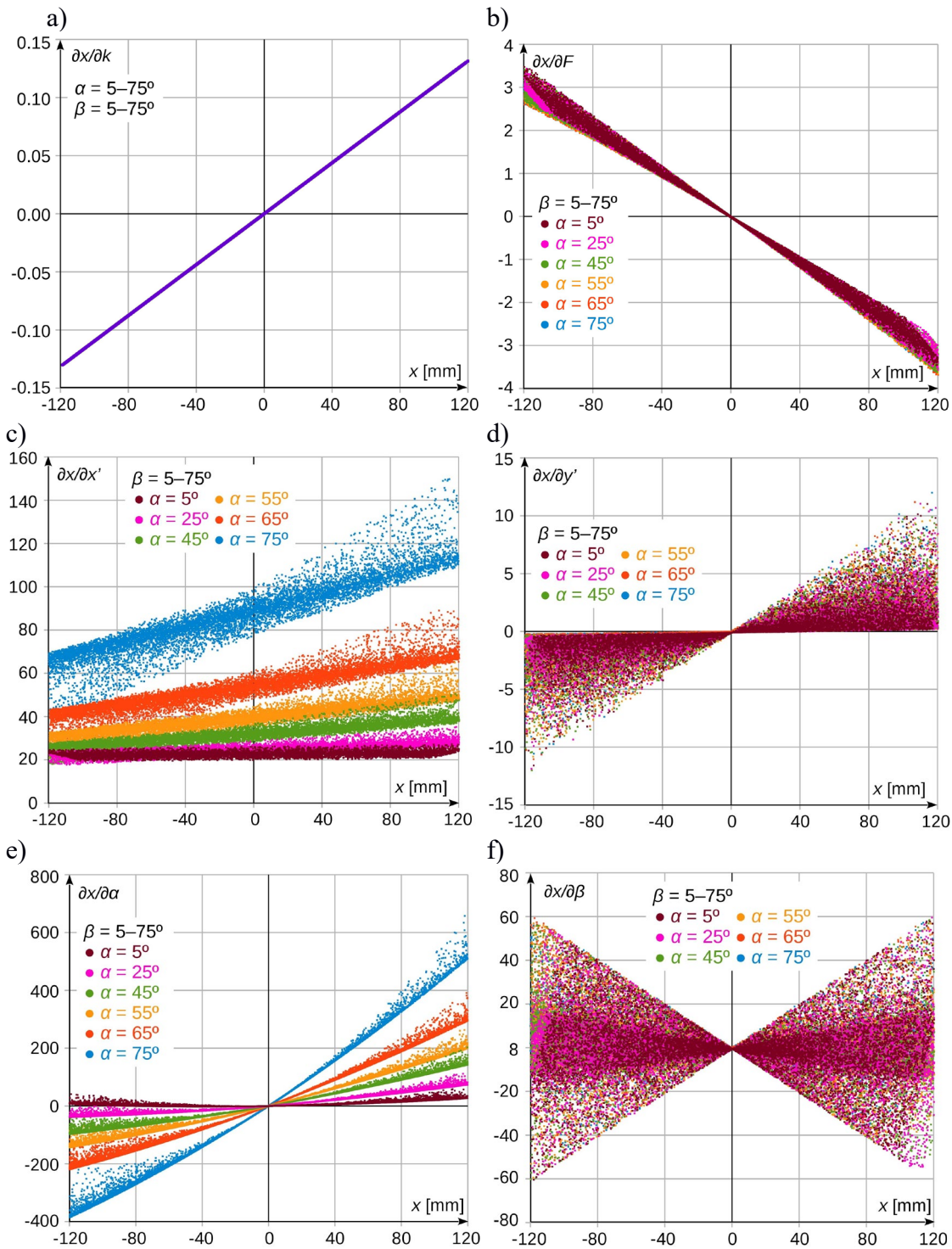
Fig. 9. Sensitivity coefficients for measurements in horizontal axis in sidelong measurement variant, where: a) measurement of distance k; b) measurement of distance F; c) measurement of point position on matrix surface in horizontal axis x'; d) measurement of point position on matrix surface in vertical axis y'; e) measurement of angle α; f) measurement of angle β

Analogously, the sensitivity coefficients in the vertical axis are given by the following formulae (33 – 38):

- measurement of the k distance:

$$\frac{\partial y}{\partial k} = \frac{y' + x' \cdot \sin\beta \cdot \tan\alpha}{F \cdot \cos\beta - y' \cdot \sin\beta - x' \cdot \tan\alpha} \quad (33)$$

- measurement of the F distance:

$$\frac{\partial y}{\partial F} = \frac{(y' + x' \cdot \sin\beta \cdot \tan\alpha) \cdot (y' \cdot \sin\beta + x' \cdot \tan\alpha - k \cdot \cos\beta)}{(F \cdot \cos\beta - y' \cdot \sin\beta - x' \cdot \tan\alpha)^2} \quad (34)$$

- measurement of the position of a point on the matrix surface in the horizontal axis x':

$$\frac{\partial y}{\partial x'} = \frac{(k - F) \cdot \tan\alpha \cdot \cos\beta \cdot (F \cdot \sin\beta + y' \cdot \cos\beta)}{(F \cdot \cos\beta - y' \cdot \sin\beta - x' \cdot \tan\alpha)^2} \quad (35)$$

- measurement of the position of a point on the matrix surface in the vertical axis y':

$$\frac{\partial y}{\partial y'} = \frac{(k - F) \cdot \cos\beta \cdot (F - x' \cdot \cos\beta \cdot \tan\alpha)}{(F \cdot \cos\beta - y' \cdot \sin\beta - x' \cdot \tan\alpha)^2} \quad (36)$$
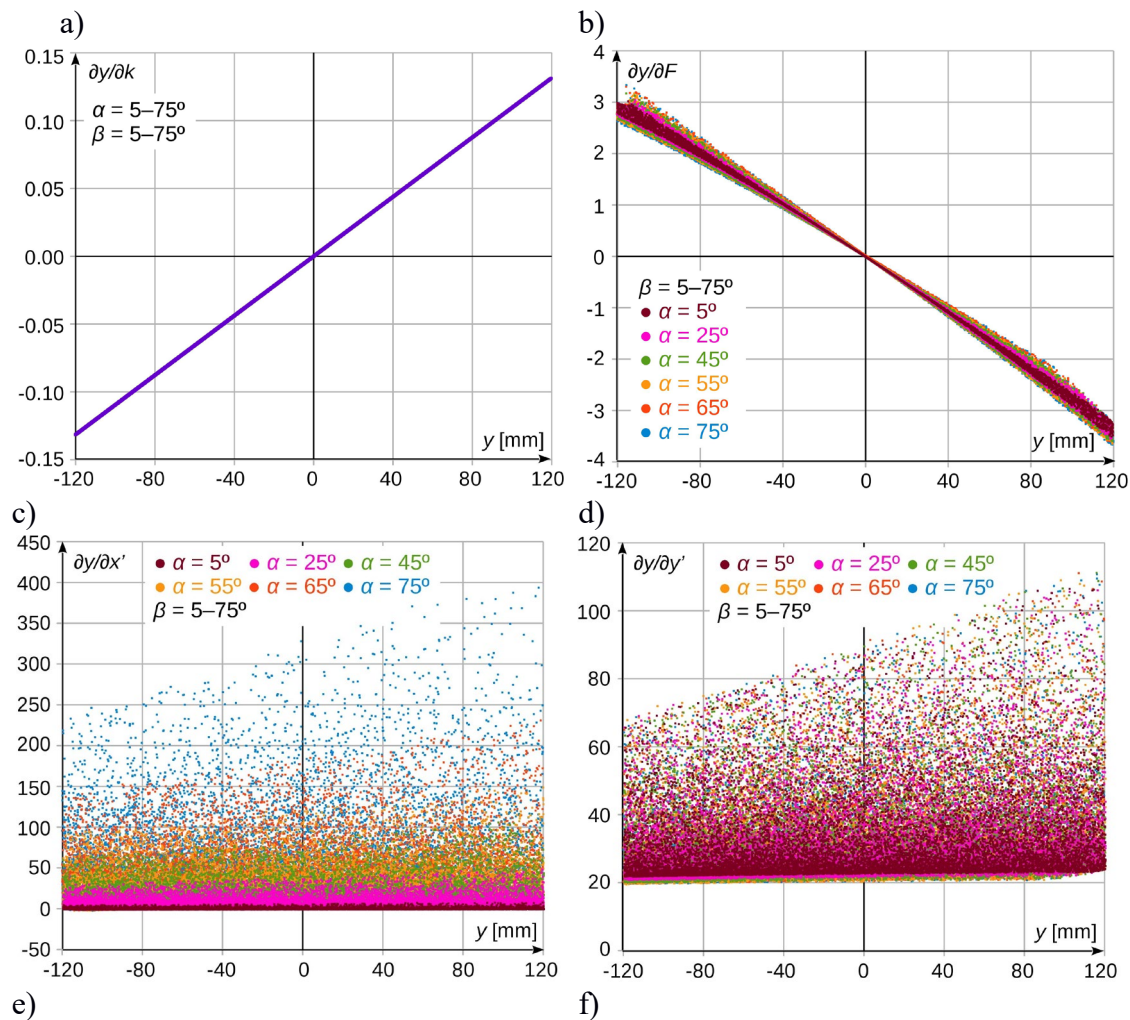
- measurement of the α angle:

$$\frac{\partial y}{\partial \alpha} = \frac{(k - F) \cdot x' \cdot \cos\beta \cdot \sec^2\alpha \cdot (F \cdot \sin\beta + y' \cdot \cos\beta)}{(F \cdot \cos\beta - y' \cdot \sin\beta - x' \cdot \tan\alpha)^2} \quad (37)$$

- measurement of the β angle:

$$\frac{\partial y}{\partial \beta} = \frac{(k - F) \cdot [x' \cdot \tan\alpha \cdot (F - \cos\beta \cdot \tan\alpha) + y' \cdot (y' \cdot \cos\beta + F \cdot \sin\beta)]}{(F \cdot \cos\beta - y' \cdot \sin\beta - x' \cdot \tan\alpha)^2} \quad (38)$$

For the values of partial measurements given in Table 1, the values of sensitivity coefficients during the measurement of vertical displacements for the sidelong measurement variant have been shown in Fig. 10.
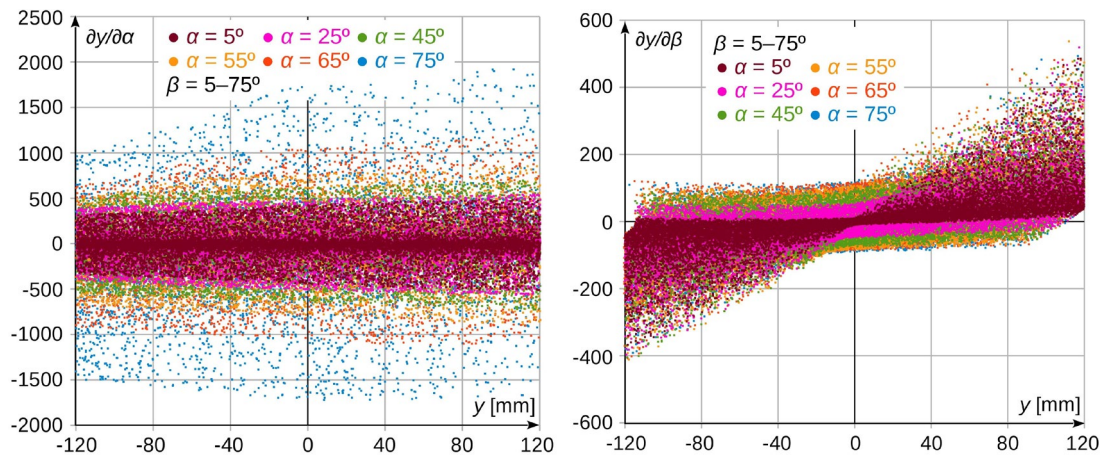
Fig. 10. Sensitivity coefficients for measurements in vertical axis in sidelong measurement variant, where: a) measurement of distance k; b) measurement of distance F; c) measurement of point position on matrix surface in horizontal axis x'; d) measurement of point position on matrix surface in vertical axis y'; e) measurement of angle α; f) measurement of angle β

4.2. Analysis of spatial configuration influence on measurement uncertainty

The analysis of obtained sensitivity coefficient results shows that, depending on the measurand, their values are radically different, starting from small ones, i.e. below one (measurement of distance k), up to very big ones, reaching even 2000 (measurement of angle α for measurements of vertical displacements in sidelong measurement variant). Apart from that, it can be observed that the values of some coefficients are independent of, or only slightly dependent on the adopted measurement variant (distances k and F), whereas the values of some other coefficient depend on the variant to a great extent (e.g. measurement of the image position on the camera matrix x' and y'). What is more, it can be observed that the value of the sensitivity coefficient does not only depend on the chosen way of measurement, i.e. the en face, the side or the sidelong one but, within a given variant, the values of angles α and β are of great importance. Due to the fact that measurement dependencies are reducing in their character, i.e. by introducing the angle value $\beta = 0$ into the dependence for sidelong measurement, we obtain dependencies for side measurement, while by zeroing both angle values we obtain dependencies for en face measurement, it should be assumed that the obtained values of measurement uncertainty, for α and β angles moving towards zero, will also approach reference values, namely those obtained for the en face measurement.

In accordance with the principles of uncertainty propagation, the standard uncertainty for displacements in the horizontal axis for en face measurement variant will be given by a dependence (39):

$$u(x) = \sqrt{\left(\frac{\partial x}{\partial x'}\right)^2 \cdot u(x')^2 + \left(\frac{\partial x}{\partial k}\right)^2 \cdot u(k)^2 + \left(\frac{\partial x}{\partial F}\right)^2 \cdot u(F)^2} \ (39)$$

An analogous dependence for the horizontal axis is given as (40):

$$u(y) = \sqrt{\left(\frac{\partial y}{\partial y'}\right)^2 \cdot u(y')^2 + \left(\frac{\partial y}{\partial k}\right)^2 \cdot u(k)^2 + \left(\frac{\partial y}{\partial F}\right)^2 \cdot u(F)^2} \ (40)$$

Taking into consideration the values of partial measurements together with uncertainties, as given in Table 1, the standard uncertainty in measurement of the position of a contact wire for the reference variant, i.e. the en face measurement, has been shown in Fig. 11. As the system is symmetrical, these results are relevant for both the horizontal and vertical displacement axis.
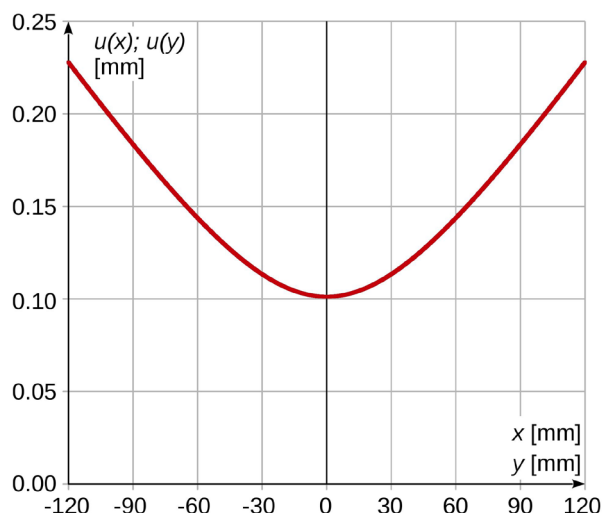
Fig. 11. Standard uncertainty for en face measurement – reference value

As shown in Fig. 11, the value of uncertainty depends on the current displacement of the measured object in relation to the zero position. The highest values of standard uncertainty, equal $u(x)_{max} = u(y)_{max} = 0.23$ mm appear for extreme measurement values (-120 or 120 mm). The obtained relative value of standard uncertainty for extreme measurement values, not exceeding 0.2%, is a very good result, taking into consideration the workshop character of the measurement and the fact that standard measurement instruments have been used to establish partial values.

Measurements for the side variant are characterised by a higher level of uncertainty, due to the introduction of an additional partial measurement of the α angle.

For this measurement variant the dependence for standard uncertainty in horizontal axis has the form following (41):

$$u(x) = \sqrt{\left(\frac{\partial x}{\partial x'}\right)^2 \cdot u(x')^2 + \left(\frac{\partial x}{\partial k}\right)^2 \cdot u(k)^2 + \left(\frac{\partial x}{\partial F}\right)^2 \cdot u(F)^2 + \left(\frac{\partial x}{\partial \alpha}\right)^2 \cdot u(\alpha)^2} \text{ (41)}$$

Respectively for the vertical axis standard uncertainty will be given by the formula (42):

$$u(y) = \sqrt{\begin{array}{l}\left(\frac{\partial y}{\partial y'}\right)^2 \cdot u(y')^2 + \left(\frac{\partial y}{\partial x'}\right)^2 \cdot u(x')^2 + \left(\frac{\partial y}{\partial k}\right)^2 \cdot u(k)^2 + \\ + \left(\frac{\partial y}{\partial F}\right)^2 \cdot u(F)^2 + \left(\frac{\partial y}{\partial \alpha}\right)^2 \cdot u(\alpha)^2\end{array}} \quad \text{(42)}$$

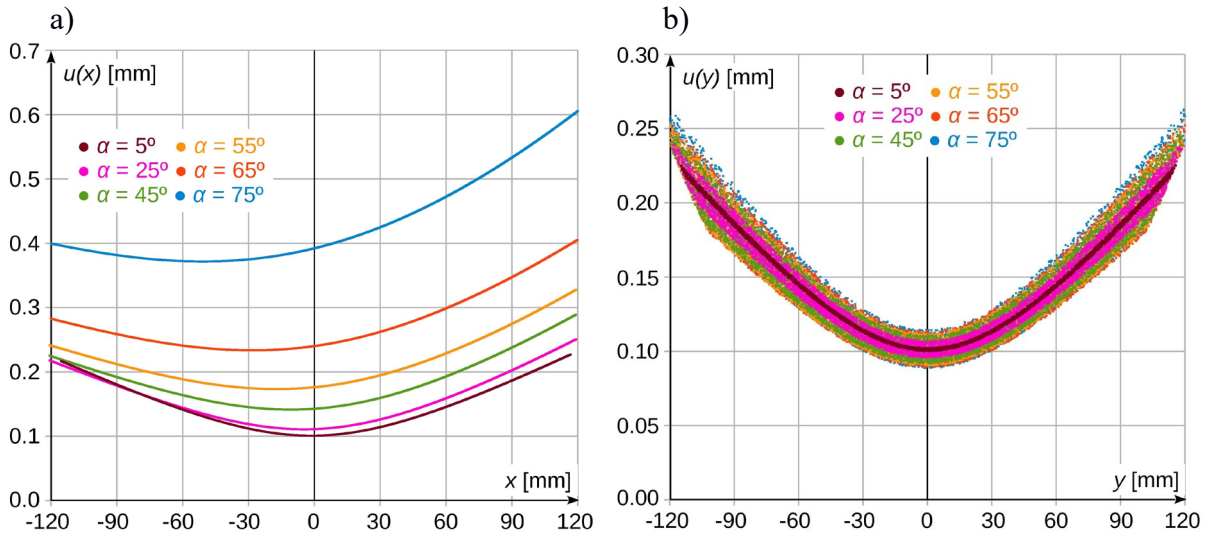The obtained dependencies for partial measurements from Table 1 have been presented graphically in Fig. 12.

Fig. 12. Standard uncertainties for measurements in side variant, where: a) uncertainty of horizontal displacements $u(x)$; b) uncertainty of vertical displacements $u(y)$

As shown in Fig. 12, the measurement uncertainty for vertical displacements depends on the value of angle α only to a small degree, and, with regard to value, practically does not differ from the level of uncertainty for the reference configuration (level increase $u(y)_{max}$ from 0.23 to 0.27 mm). The influence of the α angle value is, on the other hand, important for measurements of displacements in the horizontal axis. The higher the angle value, the more the uncertainty value increases. Rapid increase of its level appears for angle values higher than approximately $\alpha > 50°$. The dependence of maximum uncertainty value obtained for measurements in both displacement axes has been shown in Fig 13.
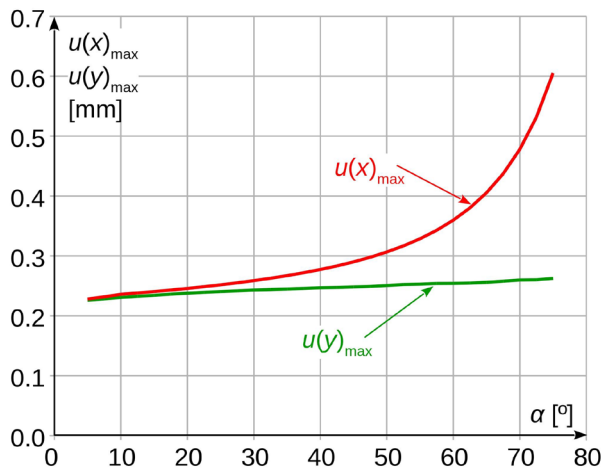

Fig. 13. Maximum values of standard uncertainties depending on α angle value for side measurement variant

For the sidelong measurement variant, the standard uncertainty of results depends on mutual combination of α and β angle values. Thus, the dependence for standard measurement uncertainty in the horizontal and vertical axes will be defined accordingly (43, 44):

$$u(x) = \sqrt{\begin{array}{l} \left(\frac{\partial x}{\partial x'}\right)^2 \cdot u(x')^2 + \left(\frac{\partial x}{\partial y'}\right)^2 \cdot u(y')^2 + \left(\frac{\partial x}{\partial k}\right)^2 \cdot u(k)^2 + \\ + \left(\frac{\partial x}{\partial F}\right)^2 \cdot u(F)^2 + \left(\frac{\partial x}{\partial \alpha}\right)^2 \cdot u(\alpha)^2 + \left(\frac{\partial x}{\partial \beta}\right)^2 \cdot u(\beta)^2 \end{array}} \quad (43)$$

$$u(y) = \sqrt{\left(\frac{\partial y}{\partial y'}\right)^2 \cdot u(y')^2 + \left(\frac{\partial y}{\partial x'}\right)^2 \cdot u(x')^2 + \left(\frac{\partial y}{\partial k}\right)^2 \cdot u(k)^2 + \\ + \left(\frac{\partial y}{\partial F}\right)^2 \cdot u(F)^2 + \left(\frac{\partial y}{\partial \alpha}\right)^2 \cdot u(\alpha)^2 + \left(\frac{\partial y}{\partial \beta}\right)^2 \cdot u(\beta)^2} \quad (44)$$

The results obtained for displacements in the horizontal axis for partial measurements from Table 1 have been presented in Fig. 14.
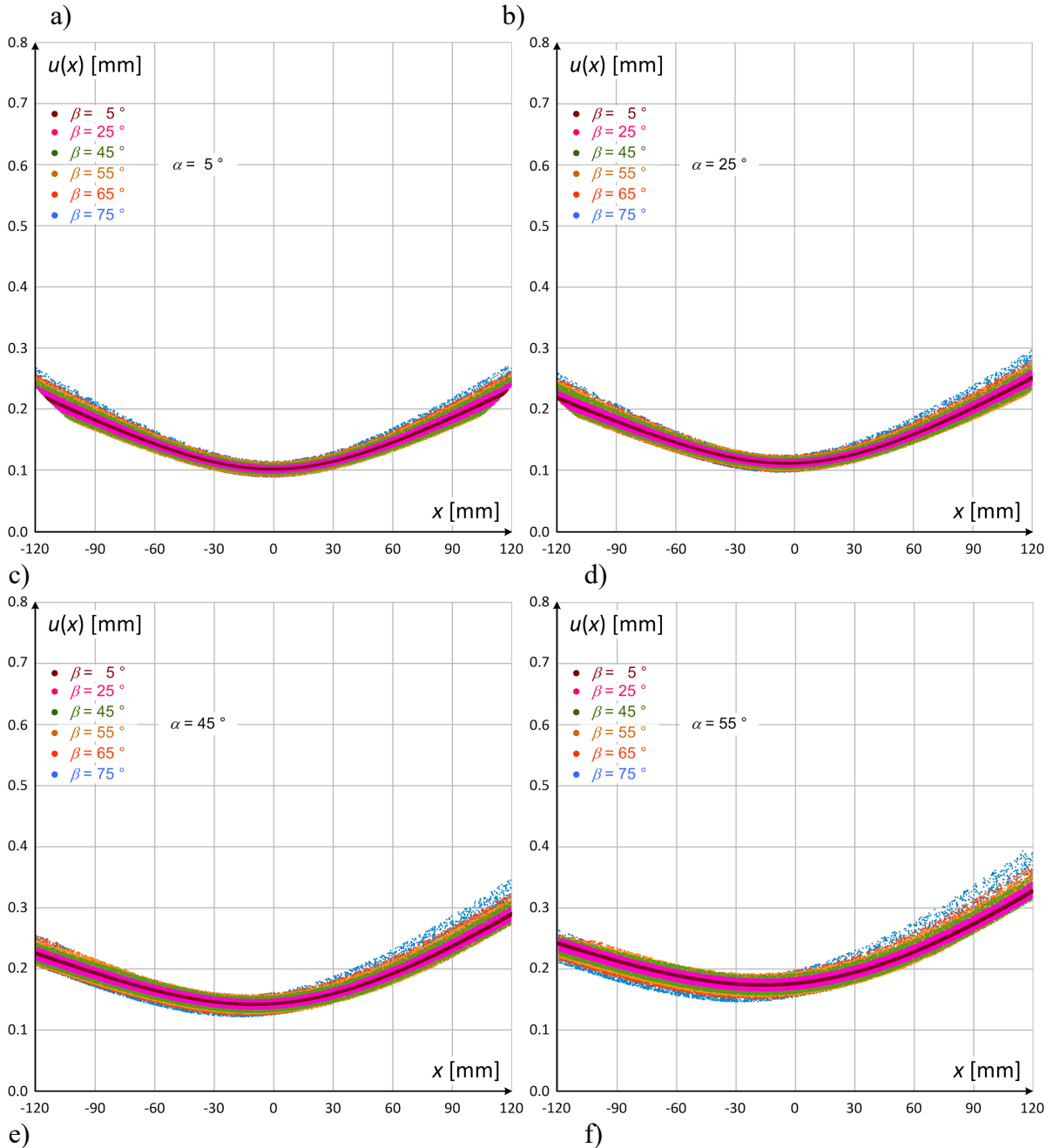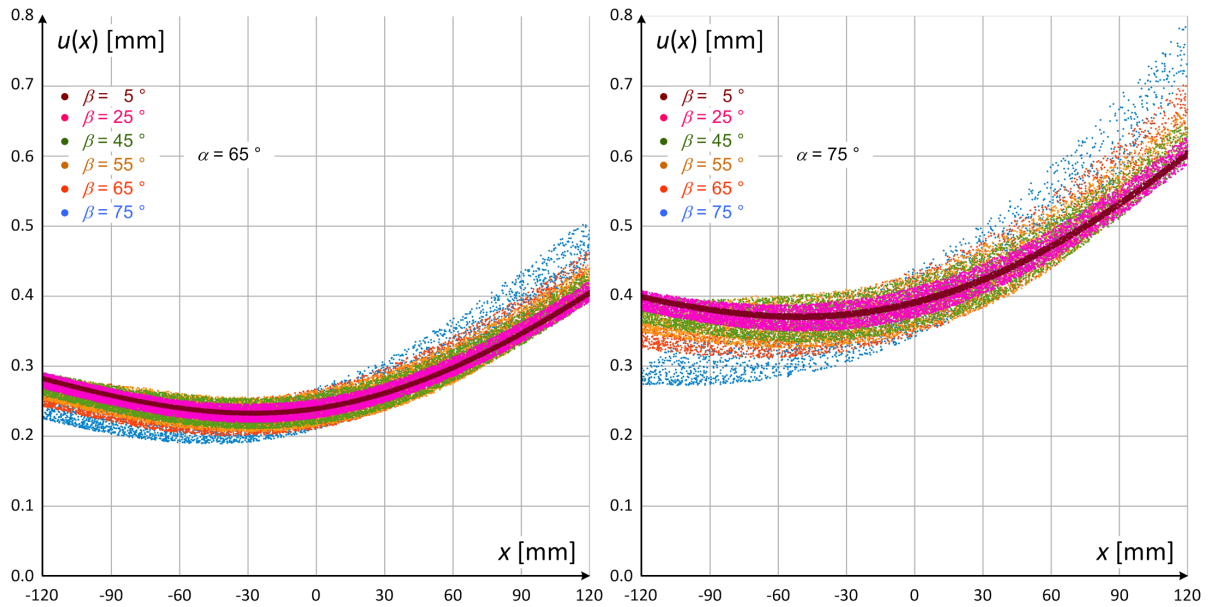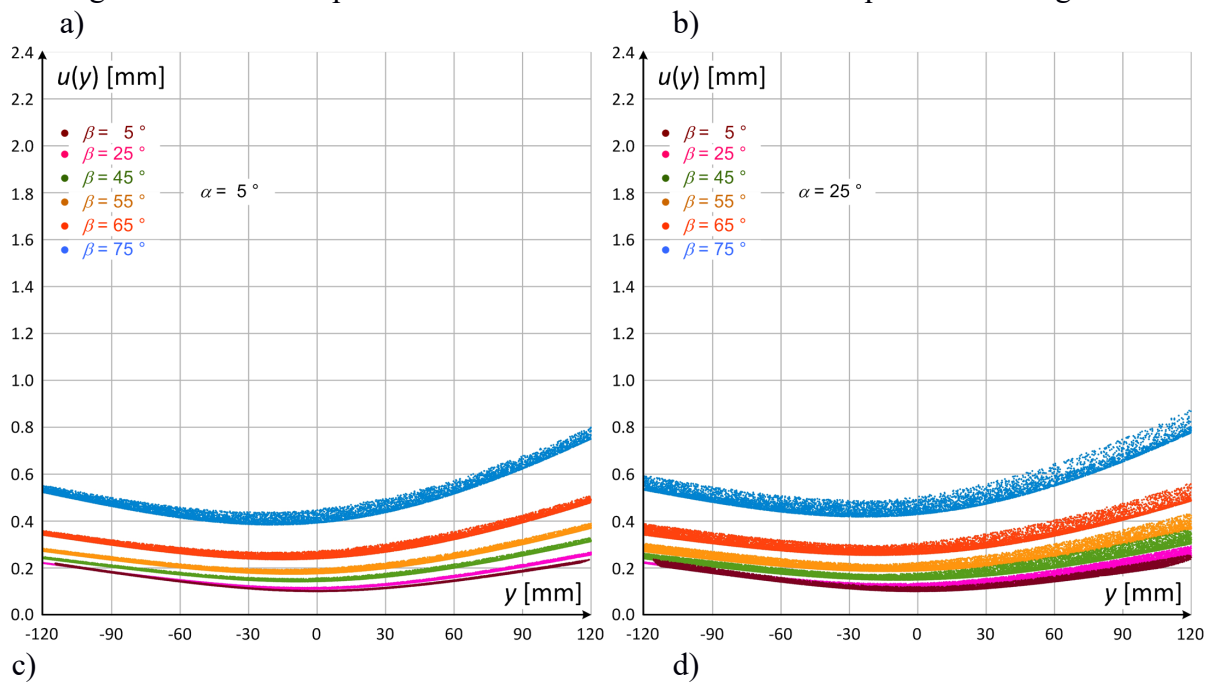
Fig. 14. Standard uncertainty of horizontal displacement measurements *u(x)* in sidelong variant, where: a) α = 5º; b) α = 25º; c) α = 45º; d) α = 65º; e) α = 75º

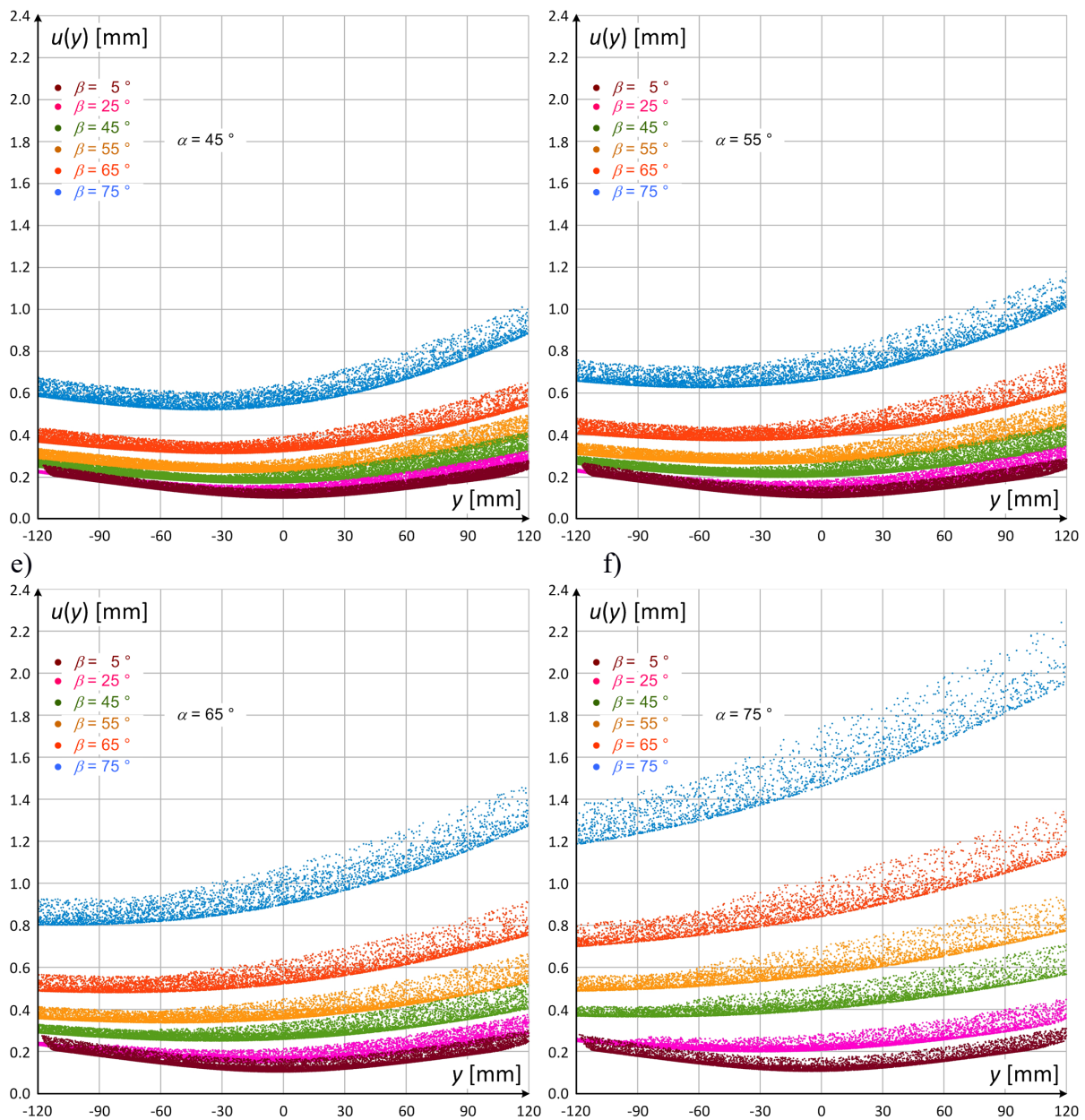Analogous results for displacements in the vertical axis have been presented in Fig. 15.

Fig. 15. Standard uncertainty of vertical displacement measurements $u(y)$ in sidelong variant, where: a) $\alpha = 5°$; b) $\alpha = 25°$; c) $\alpha = 45°$; d) $\alpha = 55°$; e) $\alpha = 65°$; f) $\alpha = 75°$

When analysing the results shown in Fig. 14 and 15, it can be observed that in the case of horizontal measurements the α angle is the dominating factor which determines the uncertainty value. For a given value of this angle, the change of angle β within a wide range does not result in any significant change of measurement uncertainty. For vertical displacements a change within a wide range of α angle value does not significantly affect the uncertainty value only in the situation where angle β is smaller than 30°. At bigger values of the β angle, changes in the values of both angles have significant influence on the uncertainty results. Therefore it can be said that, practically, the resultant value of measurement uncertainty in the case of horizontal displacements depends solely on the value of angle α, while in vertical measurements it is affected by the value of both angles, particularly if angle β is bigger than 30°. Maximum uncertainty values for horizontal and vertical displacements, dependent on the values of angles α and β have been shown in Fig 16.
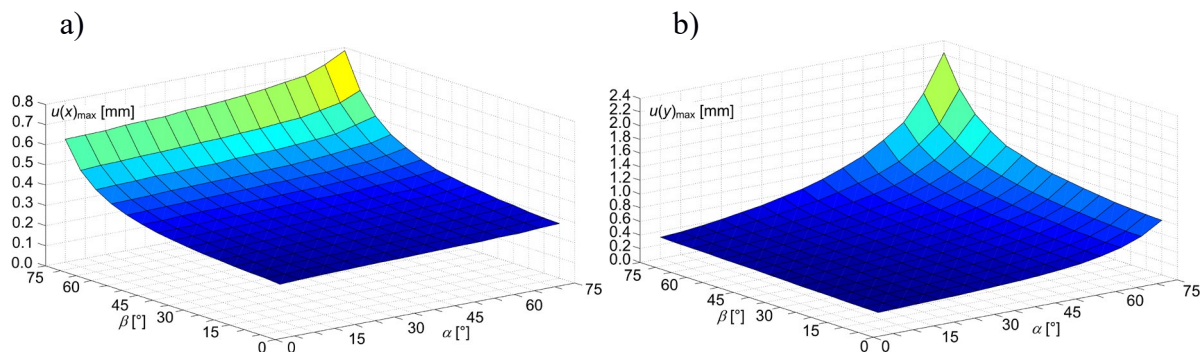
Fig. 16. Maximum uncertainty values for sidelong measurement variant, where: a) horizontal displacements; b) vertical displacements

4.3. Defining acceptable limit values of measurement uncertainty

Defining the acceptable level of measurement uncertainty depends, first and foremost, on the purpose for which such measurements are performed. There are different requirements for workshop measurements, laboratory measurements and calibration measurements.

Measurements of displacements of contact wire or other elements of the catenary may be performed, for example, for the purposes of controlling and monitoring the cooperation between current collectors and the contact line. Measurements can also be used to verify conceptual designs for new types of overhead contact line. The performed measurements may therefore belong to the area of engineering workshop measurements, which do not require a high level of precision, or may be used in research, in which case the required level of precision is higher. It was therefore concluded that relative extended uncertainty at the level of 1.5% of the maximum measurement scope will be, in the discussed case, perfectly adequate for workshop measurements, while in the case of research measurements the level of uncertainty should be twice smaller, i.e. it should not exceed 0.75%. Therefore, for the considered measurement scope, which is ±120 mm in both displacement axes, the allowed value of extended uncertainty in workshop measurements will be (45):

$$U(x,y)_{max} = \frac{120 \cdot 1.5}{100} = 1.8 \ mm \ (45)$$

For the standard value of the coverage factor $k_e = 2$ the permissible level of standard uncertainty will be (46):

$$u(x,y)_{max} = \frac{U(x,y)_{max}}{k_e} = \frac{1.8}{2} = 0.9 \ mm \ (46)$$

In the case of measurements performed for research purposes, the permissible uncertainties will be twice smaller.

4.4. Defining the range of changes in spatial parameters with regard to the allowed uncertainty level

Taking into consideration the criterion defined in p. 4.3. and analysing the results presented in Fig. 13 and 16, it can be concluded that for the side measurement variant, for the entire range of changes in the value of angle α, standard measurement uncertainty meets the requirements set for workshop measurements. The requirements for research measurements are met when the α angle is smaller than 68º.

For the sidelong measurement variant the analysis is a bit more complex. The range of changes in the values of angles α and β, together with the marked areas where the uncertainty criterion is fulfilled for both research and workshop measurements has been shown in Fig. 17.
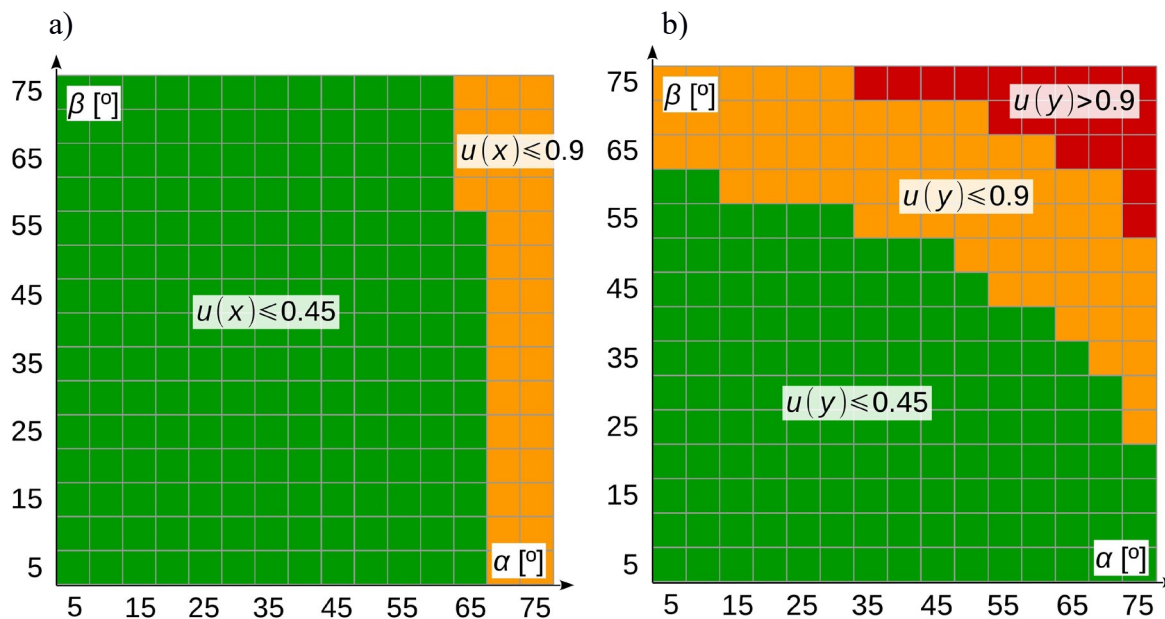
Fig. 17. Range of changes in value of angles α and β, with marked areas for which maximum uncertainty value criterion is fulfilled for research and workshop measurements, where: a) horizontal displacement measurement uncertainty $u(x)$; b) vertical displacement measurement uncertainty $u(y)$

As shown by the results, a satisfactory level of uncertainty for research measurements is achieved for angles smaller than 45 degrees. If the measurement conditions make it necessary for one of the angles to be bigger, then the second angle must be smaller (e.g. combination $\alpha = 70°$, $\beta = 30°$). Workshop measurements allow for much greater freedom with regard to determining the spatial configuration of the stand. Only an extremely unfavourable variant (e.g. $\alpha = \beta = 65°$) will result in the assumed permissible level of measurement uncertainty being exceeded.

5. Laboratory research results – verification of theoretical assumptions

The discussion concerning the influence of spatial configuration on the uncertainty of visual measurement has been subjected to verification by way of experiment. A laboratory stand, which allows for recording circular motion of an object whose dimension is 1 cm, has been created for that purpose. Such dimension is characteristic with regard to measurements and diagnostics of overhead contact line, which is usually constructed from contact wires and a support cable, whose cross-sections are approximately circular, and whose diameter ranges from 10 to 16 mm. In the case of contact wires the dimensions also depend on the degree of their wear.

The measurements were performed for all three variants of spatial configuration, i.e. en face, side and sidelong ones. In all the situation the constant distance of the camera and the reproduction ration for the values given in Table 1 were maintained. The measurements in the side variant were performed for angle $\alpha = 25.250°$, with standard uncertainty equal $u(\alpha) = 0.029°$. The measurements in the sidelong variant were performed for angles $\alpha = 33.917°$ with standard uncertainty $u(\alpha) = 0.029°$, and $\beta = 19.560°$ with standard uncertainty $u(\beta) = 0.058°$.

A block diagram of the stand for side measurement variant has been shown in Fig. 18. A reflective element, a modelling element of the contact line, has been placed on a flat bar and set in circular motion with the use of a servo drive with DC motor. The drive operates in speed regulator mode, in a closed feedback loop, with encoder measurement of the position and the

angular velocity. The distance between the reflective element and the motor shaft axis was established at the constant level of 101.920 ± 0.023 mm. The movement of the object is recorded with the use of high-speed 2D camera equipped with Camera Link interface. The whole data stream is registered in a PC computer with the use of a frame grabber. This unit, apart from acquisition of measurement data, is also capable of processing them, with the use of a dedicated application.
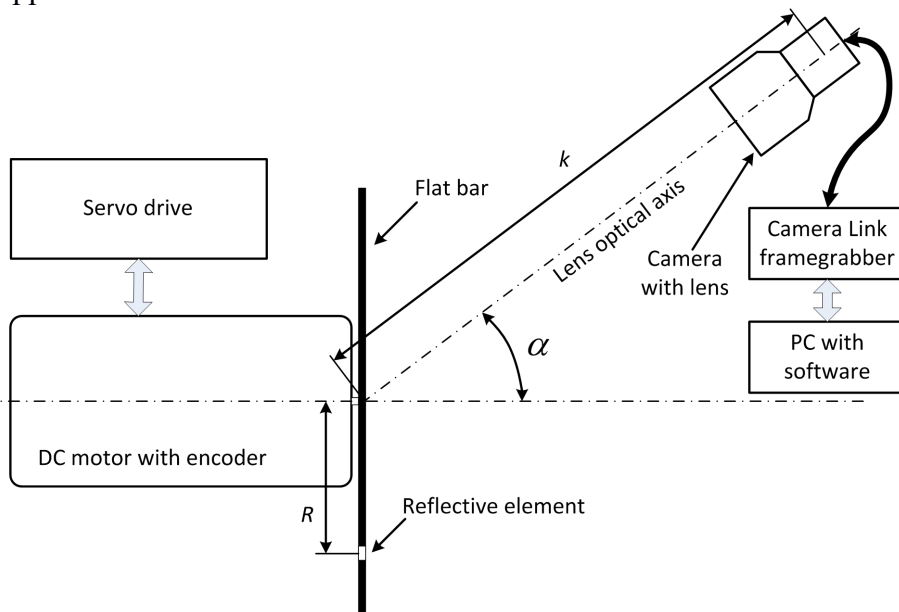

Fig. 18. Block diagram of laboratory measurement stand – side variant

For the en face configuration, it is possible to observe the movement of the reflective object in uniform circular motion, following the circle with constant radius R. In the case of measurements with α and/or β different from zero, due to trapezoidal distortions, the movement trajectory assumes the shape of an ellipse. Thanks to the algorithm for data processing, it is possible to obtain the result in a form of a circle. For all configurations the extended uncertainties of position measurements $U(x)$ and $U(y)$ were established, with the coverage factor k_e equal 2. The analysis of data, with the use of the Least-Square Fitting Algorithm was also performed. In the case of a circle, based on the collected data, the radius and the coordinates of the circle are established through minimising the function of the objective defined as (47):

$$J(x_0, y_0, R) = \Sigma\left(\sqrt{(x_i - x_0)^2 + (y_i - y_0)^2} - R\right)^2 \quad (47)$$

where: x_0 – the x-coordinate of the centre of the circle, y_0 – the y-coordinate of the centre of the circle, R – radius of the circle, x_i, y_i – ith data point.

The minimisation is performed with the use of the Levenberg-Marquardt algorithm. The measure of adapting the data to a circle with certain parameters is the sum of the squares of elements vector of residuals in numerical analysis point of view. The results of the conducted analysis, for an object moving along a circle with the radius R = 101.920 ± 0.023 mm have been presented in Table 2.

Table 2. Results of processing with the Least Square Method adjustment algorithm

	radius	residue
En face measurement	101.90	0.63
Side measurement	101.71	3.19
Sidelong measurement	101.84	3.90

The results showing the position of the object on the *xy* plane, recorded for the three variants of camera position, together with marked extended uncertainties, have been presented in Fig. 19. Constant distance *k* and radius *R* were maintained during the measurements.
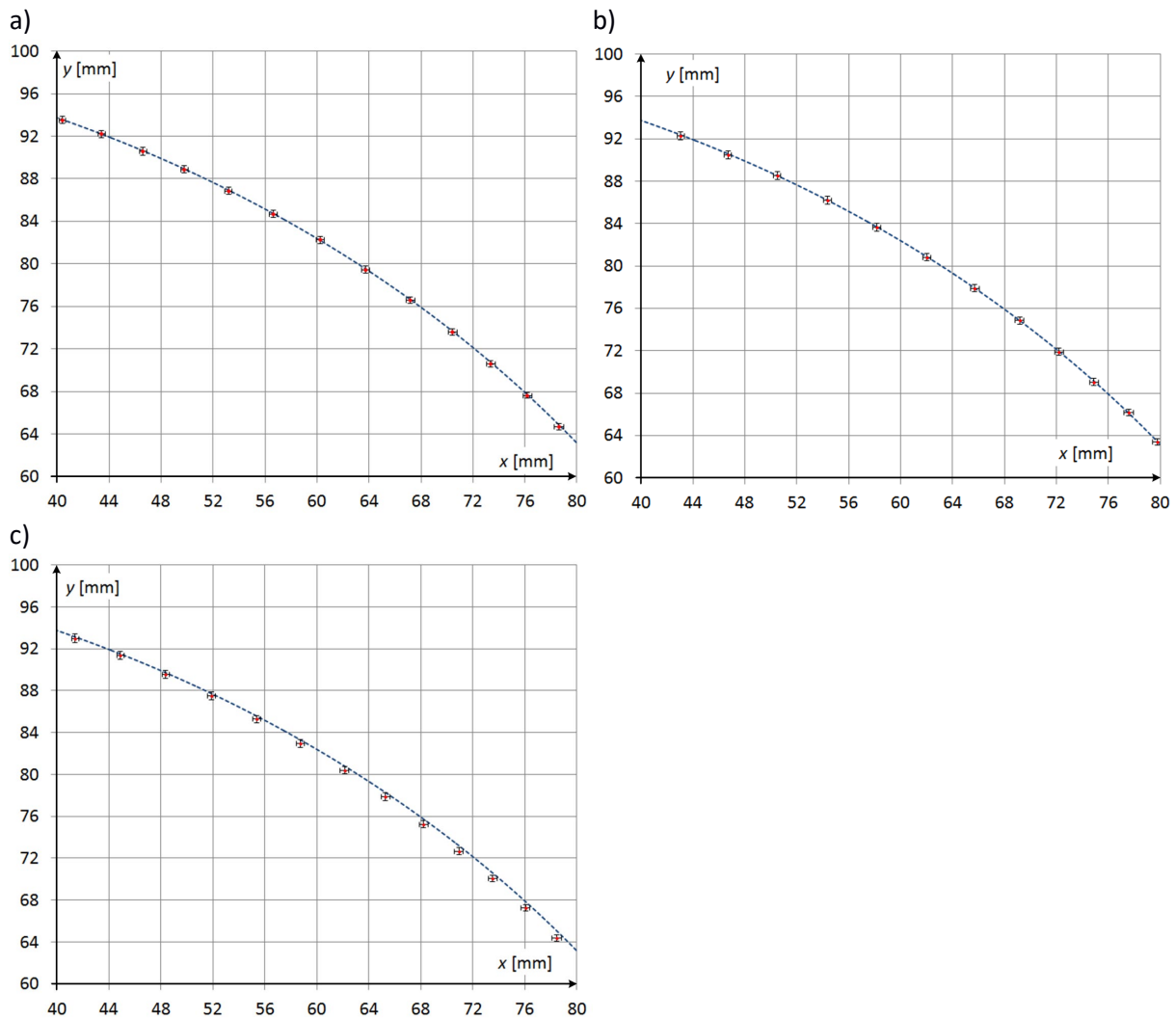
a)

b)

c)

Fig. 19. Results of measuring position of object in circular motion, together with extended uncertainties $U(x)$ and $U(y)$ for radius $R = 101.920$ mm: a) en face measurement, b) side measurements, c) sidelong measurement

The presented analysis shows that the differences between the obtained measurement results and the real position of the measured object fall within the permissible uncertainty arising from spatial configuration of the measurement stand.

6. Examples of measurement results for measurements performed on a real object

In order to test the method in real laboratory measurement conditions, the vibrations of a catenary contact wire were measured at a stand, whose diagram is presented in Fig. 20.
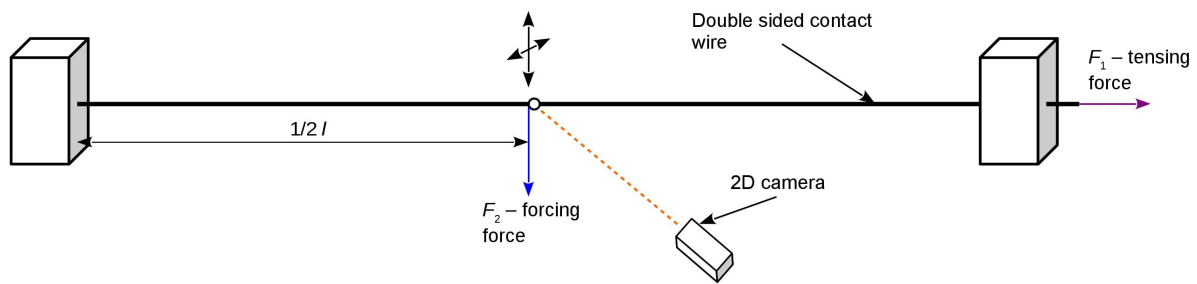
Fig. 20. Block diagram of measurement stand for examining vibrations of catenary contact wire

A bilaterally attached section of a contact wire with the length $l = 28.8$ m was tensioned with the force $F_1 = 10$ kN and stimulated to vibrate by applying pressure force operating in vertical axis, $F_2 = 100$ N. The vibration measurements were performed in the sidelong variant for a geometrical configuration resulting from partial measurement results presented in Table 3.

Table 3. Results of partial measurements of configuration of a laboratory stand for overhead contact line research

No.	Measured value	Measurement instrument	Measurement result	Standard uncertainty
1	Distance k between image plane and object plane	1st class accuracy gauge Hultafors CC10M B	2784.50 mm	±0.24 mm
2	Distance F between main lens plane and image plane	Indirect measurement	87.75 mm	±0.15 mm
3	Angle α between camera and contact wire	Precise mechanical protractor FWP MKMb	52.750º	±0.029º
4	Angle β of camera inclination in relation to level	Inclinometer ACS-080-2-SC00-HE2-2W	26.800º	±0.058º

Due to the obtained contact wire displacements, the useful measurement range was narrowed to ±6 mm in the horizontal axis and ±80 mm in the vertical axis. A sample measurement result has been presented in Fig. 21.
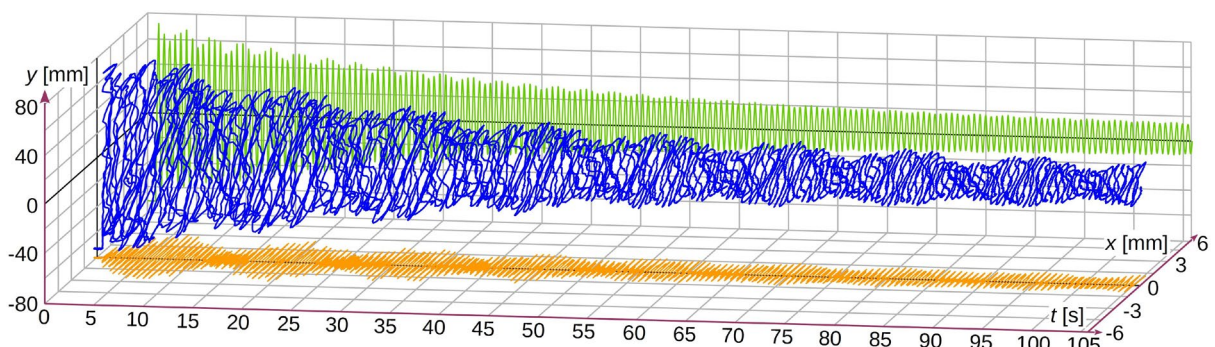
Fig. 21. Flow of free vibrations of contact wire caused by application of irregular pressure force

The analysis of measurement uncertainty for the discussed laboratory test showed that, for the assumed coverage factor k_e equal 2, the maximum extended uncertainty for horizontal and vertical displacement measurements is $U(x)_{max} = 0.46$ mm, and $U(y)_{max} = 0.47$ respectively. Taking into consideration the maximum recorded value of vertical displacements, the obtained

extended uncertainty was at the level of 0.59%, which complies with the assumed, recommended level for research measurements.

7. Summary

It has been theoretically proved in the consideration presented above that, for the discussed issue, i.e. measurement of displacements of contact line elements with the use of contact-less visual method, it is possible to obtain the level of measurement uncertainty, which is satisfactory in everyday research and engineering practices. It has been shown that such level is obtainable even with the use of typical laboratory measurement instruments for partial measurements. It has also been concluded that, for more complex spatial configurations of a research stand (the side and sidelong measurements) the uncertainty level of the obtained results deteriorated slightly in relation to the reference variant (the en face measurement), provided that the values of angle α or of angles α and β do not exceed the level of approximately 45-50º. For higher angle values it is necessary to be more careful and check every time if the obtained uncertainty level is satisfactory for the given measurement requirements. The theoretical discussion was verified at a laboratory stand, reconstructing in a known way the movement of an object within the range typical for a catenary contact wire. The correctness of the above-mentioned discussion was then confirmed through performing laboratory measurements on a real object.

8. Final conclusions

Remote optical measurements, performed with the use of an image camera, constitute a modern alternative for measurements performed with the use of traditional measurements methods. They are also a competition for some modern methods using, for example, laser distance meters. Their advantage is the possibility to perform a measurement from a certain distance, without interference or interaction with the measured object. In situations where the application of traditional methods is very difficult or impossible (e.g. measuring the displacement of catenary contact wires, caused by current collectors, conducted in real conditions on an operating railway), optical measurements are often the only possible way to realise the measurement. However, the level of obtained uncertainty always has to be taken into consideration, as the measurement characterised by over-high uncertainty level are not robust and, as a result, unreliable and worthless. The conducted theoretical analysis and verification tests have shown that, for the considered spatial configurations of a measurement stand, the obtained level of uncertainty guarantees good quality of measurement results, provided that certain conditions are fulfilled. However, the influence of the distance between the object and the camera on uncertainty has not been checked in the course of the research. Performance of such analyses and stipulation of uncertainty criteria for measurements performed at a greater distance will constitute the area of further research work.

[1] Pastucha, E. Catenary System Detection, Localization and Classification Using Mobile Scanning Data. Remote Sens. 2016, 8, 801. doi:10.3390/rs8100801

[2] Arastounia, M. Automated Recognition of Railroad Infrastructure in Rural Areas from LIDAR Data. Remote Sens. 2015, 7, 14916-14938. doi:10.3390/rs71114916

[3] Barmada, S., Landi, A., Papi, M., Sani, L., 2003. Wavelet multiresolution analysis for monitoring the occurrence of arcing on overhead electrified railways. Proc. Inst. Mech. Eng. Part F J. Rail Rapid Transit 217, 177–187. doi:10.1243/095440903769012885

[4] Landi, A., Menconi, L., Sani, L., 2006. Hough transform and thermo-vision for monitoring pantograph-catenary system. Proc. Inst. Mech. Eng. Part F J. Rail Rapid Transit 220, 435–447. doi:10.1243/0954409JRRT41

[5] Karakose, E., Gencoglu, M.T., Karakose, M., Aydin, I., Akin, E., 2017. A New Experimental Approach Using Image Processing-Based Tracking for an Efficient Fault Diagnosis in Pantograph-Catenary Systems. IEEE Trans. Ind. Inform. 13, 635–643. doi:10.1109/TII.2016.2628042

[6] Bruno, O., Landi, A., Papi, M., Sani, L. and Violi, A. G. Pantograph-catenary monitoring: correlation between break arcs and harmonics in the traction current. In CDROM of The World Conference Railway Research'01, Köln, Germany, 25-29 November 2001.

[7] Koyama, T., Ikeda, M., Nakamura, K., Tabayashi, S., Niwakawa, M., 2012. Measuring the contact force of a pantograph by image processing technology. pp. 189–198. doi:10.2495/CR120171

[8] Cho, C.J., Ko, H., 2015. Video-Based Dynamic Stagger Measurement of Railway Overhead Power Lines Using Rotation-Invariant Feature Matching. IEEE Trans. Intell. Transp. Syst. 16, 1294–1304. doi:10.1109/TITS.2014.2361647

[9] Cho, C.J., Park, Y., 2016. New Monitoring Technologies for Overhead Contact Line at 400 km·h−1. Engineering 2, 360–365. doi:10.1016/J.ENG.2016.03.016

[10] Zimmert G. Dynamisches Verhalten der Oberleitung für 350 km/h auf der neuen Strecke Wuhan – Guangzhou. Elektrische Bahnen 108 (2010) Heft 4 ISSN 0013-5437

[11] Vázquez, C.A.L., Quintas, M.M., Romera, M.M., 2010. Non-contact sensor for monitoring catenary-pantograph interaction, in: 2010 IEEE International Symposium on Industrial Electronics. Presented at the 2010 IEEE International Symposium on Industrial Electronics, pp. 482–487. doi:10.1109/ISIE.2010.5637852

[12] Karwowski, K., Mizan, M., Karkosiński, D., 2016. Monitoring of current collectors on the railway line. Transport 0, 1–9. doi:10.3846/16484142.2016.1144222

[13] Skibicki, J., 2013. The new version of contact-less method for localisation of catenary contact wire – theoretical assumption. Przegląd Elektrotechniczny 07/2013 pp. 100–104.

[14] Skibicki, J., Bartłomiejczyk, M., 2017. Analysis of measurement uncertainty for contact-less method used to measure the position of catenary contact wire, performed with the use of Monte Carlo method. Measurement 97, 203–217. doi:10.1016/j.measurement.2016.11.008

[15] Liu, Z., Liu, W., Han, Z., 2017. A High-Precision Detection Approach for Catenary Geometry Parameters of Electrical Railway. IEEE Trans. Instrum. Meas. PP, 1–11. doi:10.1109/TIM.2017.2666358

[16] Aydin, I., Karaköse, M., Akin, E., 2013. A Robust Anomaly Detection in Pantograph-Catenary System Based on Mean-Shift Tracking and Foreground Detection, in: 2013 IEEE International Conference on Systems, Man, and Cybernetics. Presented at the 2013 IEEE International Conference on Systems, Man, and Cybernetics, pp. 4444–4449. doi:10.1109/SMC.2013.757

[17] Hulin, B., Schubler, S., 2007. Concepts for Day-Night Stereo Obstacle Detection in the Pantograph Gauge, in: 2007 5th IEEE International Conference on Industrial Informatics. Presented at the 2007 5th IEEE International Conference on Industrial Informatics, pp. 449–454. doi:10.1109/INDIN.2007.4384799

[18] Stefano, E.D., Ruffaldi, E., Avizzano, C.A., 2016. Automatic 2D-3D vision based assessment of the attitude of a train pantograph, in: 2016 IEEE International Smart Cities Conference (ISC2). Presented at the 2016 IEEE International Smart Cities Conference (ISC2), pp. 1–5. doi:10.1109/ISC2.2016.7580747

[19] Tang, P., Jin, W., Liu, J., 2016. Railway inspection oriented foreground objects detection and occlusion reasoning for locomotive-mounted camera video, in: 2016 35th Chinese Control Conference (CCC). Presented at the 2016 35th Chinese Control Conference (CCC), pp. 10144–10149. doi:10.1109/ChiCC.2016.7554962

[20] Judek S., Jarzebowicz L., 2016. Analysis of Measurement Errors in Rail Vehicles' Pantograph Inspection System. Elektronika Ir Elektrotechnika. Vol 22, No 3 (2016), pp. 20–23. doi: 10.5755/j01.eie.22.3.15309

[21] Yang, Q., Sun, C., Wang, P., Li, W., Liu, X., 2015. Distortion correction for the orthogonally-splitting-imaging pose sensor. Opt. Laser Technol. 69, 160–171. doi:10.1016/j.optlastec.2014.12.029

[22] Lavatelli, A., Zappa, E., 2016. Modeling Uncertainty for a Vision System Applied to Vibration Measurements. IEEE Trans. Instrum. Meas. 65, 1818–1826. doi:10.1109/TIM.2016.2541359

[23] Aydin, I., 2015. A new approach based on firefly algorithm for vision-based railway overhead inspection system. Measurement 74, 43–55. doi:10.1016/j.measurement.2015.07.022

[24] Davies, E.R. (Ed.), 2005. Machine Vision, in: Machine Vision (Third Edition), Signal Processing and Its Applications. Morgan Kaufmann, Burlington, p. i. doi:10.1016/B978-0-12-206093-9.50039-3

[25] Schreve, K., 2014. How accurate can a stereovision measurement be?, in: 15th International Workshop on Research and Education in Mechatronics (REM). Presented at the 15th International Workshop on Research and Education in Mechatronics (REM), pp. 1–7. doi:10.1109/REM.2014.6920229

[26] Dong, T., Hua, D., Li, Y., Ni, J., 2014. Measuring principle of vertical target density based on single linear array CCD camera. Opt. - Int. J. Light Electron Opt. 125, 176–178. doi:10.1016/j.ijleo.2013.07.006